PCCP

ARTICLE TYPE

Cite this: DOI: 00.0000/xxxxxxxxxx

A computational study of the vibronic effects on the electronic spectra and the photophysics of aza[7]helicene†

Yanli Liu,*[a] Daniel Aranda,*[b] and Fabrizio Santoro*[b]

Received Date
Accepted Date

DOI: 00.0000/xxxxxxxxxx

We report a computational study on vibronic effects in the spectroscopy, photoinduced processes and decay back to the ground state of aza[7]helicene, a helicene with an unusually high fluorescence quantum yield (QY=0.39). In a first step, we compute and assign the absorption and electronic circular dichroism (ECD) spectra in its full frequency range from 2.7 to 5.0 eV, accounting for nonadiabatic effects. Then we compute the quantum dynamics of the cascade of ultrafast internal conversions of the highly-excited singlet states to the lowest-energy one S_1. Finally we adopt Fermi golden rule rates to compute the QY of the dye, taking into account the competition between the radiative decay and the nonradiative decays to the ground state and to the energy-accessible triplet states. We use time-dependent density functional theory (TD-DFT), including solvent (dichloromethane) effects within the polarizable continuum model, to parametrize a linear vibronic coupling (LVC) model involving the first lowest 12 singlet states and all the normal coordinates. Nonadiabatic spectra and internal conversions dynamics are then computed through wavepacket propagations with the Multilayer (ML) extension of the Multiconfigurational Time Dependent Hartree method (ML-MCTDH). We individuate the molecular vibrations playing a major role in determining the shape of the spectra and analyse the effect of inter-state couplings. At the same time we highlight a breakdown of perturbative Herzberg-Teller approaches. The computed QY is in perfect agreement with experiment and allow us to ascertain that intersystem crossings are the processes limiting the fluorescence from S_1. They involve the three lowest triplet states and are made effective by spin-orbit coupling and vibronic effects.

1 Introduction

Helicenes are fully aromatic compounds made up by ortho-fused angularly annulated aromatic rings.[1,2] They can show large optical rotation and strong Cotton effect in electronic circular dichroism (ECD).[2–6] As an example, recently reported helicene-based nanoribbons exhibit some of the largest anisotropy of the molar absorptivity ever measured in the visible for a single molecule.[7–9] Because of these properties, helicenes and their derivatives have attracted a large interest with applications in chirality sensing,[10] chiroptical materials[11] and optical devices.[12] However, their applicability to optoelectronic devices has been limited by their generally-low fluorescence quantum yield (QY),[13–15] defined as the ratio of emitted photons over absorbed photons. Experimental studies suggest that intersystem crossing (ISC) pathways of helicenes are highly accelerated with respect to the corresponding planar compounds, because in principle the helical structure allows strong mixing between singlet and triplet $\pi\pi^*$ states.[15–21] Despite this, few computational studies thoroughly investigated this issue and explicit computational predictions of the ISC rates of helicene compounds has been rarely reported so far, to the best of our knowledge.[22]

The past decades have witnessed a boom in the synthesis of [n]helicenes (where "n" is the number of ortho-fused aromatic rings) with improved QY and promising chiroptical properties. It was found that an effective way to achieve this target is to introduce polycyclic aromatic which incorporate heteroatoms[10,23–25] and in fact, a series of [n]helicenes and [n]helicene-like compounds composed of phenanthroline and heterocycles were reported.[26,27]

Recently, a special kind of aza[7]helicene (Figure 1), with a rare 6-5-6-6-6-5-6 skeleton, was synthesized by Otani et al.,[26] and showed high circularly polarized luminescence (CPL) efficiency and a high QY (0.39). The high QY of aza[7]helicene is

[a] School of Physics and Optoelectronics Engineering, Ludong University, 264025 Yantai, Shandong, PR China; E-mail: yanliliu@ldu.edu.cn
[b] CNR–Consiglio Nazionale delle Ricerche, Istituto di Chimica dei Composti Organo Metallici (ICCOM-CNR), SS di Pisa, Area della Ricerca, via G. Moruzzi 1, I-56124 Pisa, Italy. E-mail:daniel.aranda@pi.iccom.cnr.it; fabrizio.santoro@pi.iccom.cnr.it

† Electronic Supplementary Information (ESI) available: [Theory on LVC model; Convergence tests. Additional results with different solvation models. Further discussion on the estimate of QY. See DOI: 10.1039/cXCP00000x/

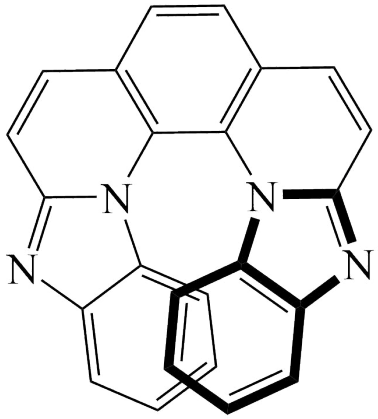

Fig. 1 Molecular structure of the (*M*)-aza[7]helicene studied in this work.

remarkable for a helicene-derivative, and it further increases in acidic conditions up to 0.80.[26]

Nowadays computational methods are routinely employed to improve our understanding of the photophysical processes of molecular systems. Accurate electronic calculations are of course mandatory, to individuate the relevant electronic states and decipher the main photophysical pathways. However, in order to achieve a direct simulation of spectral shapes, as well as, of the decay mechanisms and rates of the excited states, it is necessary to investigate the effect of the motion of the nuclear structure. On this respect, quantum nuclear effects, the so called vibronic effects, are expected to be important, but their description can be quite challenging.

In this work we show that since aza[7]helicene is rigid enough to allow a simple description of the potential energy surfaces (PESs), recent theoretical developments make nowadays possible a detailed investigation of vibronic effects on its photophysics. In a previous contribution, some of us computed the vibrationally resolved emission (EMI), and CPL spectra of aza[7]helicene, and its absorption (ABS) and ECD in the low-energy region, involving the lowest-excited singlet state S_1.[28] To that end we exploited recent time-independent and time-dependent methods for vibronic effects in cases of negligible or weak inter-state couplings. Here we present a much more extended study of the spectroscopy and photophysical properties of aza[7]helicene, explicitly addressing nonadiabatic effects. First, (i) we simulate and discuss the ABS and ECD vibronic spectra in their full wavelength range, corresponding to ∼2.5 eV, which involves 12 electronic singlet states. Second, (ii) we adopt nonadiabatic quantum dynamics (QD) to investigate the ultrafast internal conversions (IC) toward the lowest-energy singlet state, S_1. Third, (iii) we use vibronic theories within Fermi Golden Rule (FGR) approach to estimate the QY from S_1, investigating the competition between the radiative and non-radiative (IC) rates toward S_0, and the ISC rates toward the accessible triplet states.

Calculations at points (i) and (ii) requires a nonadiabatic approach where couplings among electronic states induced by nuclear motions are explicitly accounted for. While this necessity is obvious to describe population transfers between electronic states, actually it does hold also for electronic spectra. In fact, as we will show, the third band of the spectra of aza[7]helicene, falling at energies > 4 eV, arises from the contribution of ~ 8 states falling in an energy range <1 eV. These states are so close in energy that several resonances can occur when considering also vibrational states, and even tiny couplings can in principle give rise to strong mixings and exchange of intensity. We will show that in these cases the use of perturbative approaches, like Herzberg-Teller (HT) theory,[29] to introduce these effects can lead to large artefacts.[30] It is therefore necessary to resort to a fully nonadiabatic non-perturbative approach. Here we propagate vibronic wavepackets on the coupled potential energies (PESs) of the different electronic states described within a Linear Vibronic Coupling (LVC) model. The latter is parametrized with respect to Time-dependent density functional theory (TD-DFT) calculations with a maximum-overlap diabatization approach.[31] QD wavepacket propagations on so many coupled states including the effect of all relevant vibrational degrees of freedom is possible thanks to the Multilayer (ML) generalization of Multiconfigurational Time Dependent Hartree method (ML-MCTDH).[32–35]

2 Methods

2.1 Linear Vibronic Coupling Hamiltonian and Quantum Dynamics

We adopt a LVC model to deal with cases where the final electronic states of the transition are coupled. Consider a model Hamiltonian in a diabatic basis of dimension n, $|\mathbf{d}\rangle = (|d_1\rangle, |d_2\rangle, \cdots, |d_n\rangle$,

$$H = \sum_i \left(K + V_{ii}^{dia}(\mathbf{q})\right)|d_i\rangle\langle d_i| + \sum_{i,j>i} V_{ij}^{dia}(\mathbf{q})(|d_i\rangle\langle d_j| + |d_j\rangle\langle d_i|) \quad (1)$$

where K and V represent kinetic and potential terms and we use dimensionless normal coordinates $\mathbf{q}$ and conjugated momenta $\mathbf{p}$. The PESs are considered harmonic, and the normal modes and frequencies of all the excited states are approximated to the ground state ones. This means that the different PESs of the diabatic states ($V_{ii}^{dia}(\mathbf{q})$) only differ by linear terms that determine the equilibrium position. In the same way, inter-state couplings $V_{ij}^{dia}(\mathbf{q})$ $(i \neq j)$ are linear with respect to $\mathbf{q}$.

$$K = \frac{1}{2}\mathbf{p}^T\boldsymbol{\Omega}\mathbf{p} \quad (2)$$

$$V_{ii}^{dia}(\mathbf{q}) = E_i^0 + \boldsymbol{\lambda}_{ii}^T\mathbf{q} + \frac{1}{2}\mathbf{q}^T\boldsymbol{\Omega}\mathbf{q}, \quad (3)$$

$$V_{ij}^{dia}(\mathbf{q}) = \boldsymbol{\lambda}_{ij}^T\mathbf{q}. \quad (4)$$

$\boldsymbol{\Omega}$ is the diagonal matrix of the S_0 vibrational frequencies, E_i^0 and $\boldsymbol{\lambda}_{ii}$ are the ith excited state energy and gradients, respectively, and $\boldsymbol{\lambda}_{ij}$ the interstate couplings. T represents the standard transpose operation.

The vibronic wavefunction is expressed as $|\Psi(\mathbf{q},t)\rangle = \sum_i |d_i\rangle|\Psi_i(\mathbf{q},t)\rangle$ and its time evolution is computed solving the time-dependent (TD) Schrödinger Equation:

$$i\hbar\partial_t|\Psi(\mathbf{q},t)\rangle = H|\Psi(\mathbf{q},t)\rangle \quad (5)$$

Once $|\Psi(\mathbf{q},t)\rangle$ is known, it is possible to obtain the ABS and ECD vibronic spectra, according to the expression reported in the following section. At the same time, we can also analyse the time-evolution of the diabatic electronic populations which are straightforwardly computed as $P_i(t) = \langle\Psi_i(\mathbf{q},t)|\Psi_i(\mathbf{q},t)\rangle$.

The LVC Hamiltonian is parametrized with TD-DFT adopting a maximum-overlap diabatization procedure. A complete presentation of the method is described in reference[31] while a brief description is given in the ESI.

2.2 Nonadiabatic calculation of the Absorption and ECD spectra

We adopt TD expressions for the ABS and ECD spectra

$$\begin{aligned}\varepsilon(\omega) &= \mathscr{C}_\varepsilon\omega\sum_{ji}\int_{-\infty}^{\infty}dt e^{i(\omega+\omega_0)t}\langle\mathbf{0};d_j|\boldsymbol{\mu}_{gj}e^{-iHt/\hbar}\boldsymbol{\mu}_{ig}|d_i;\mathbf{0}\rangle f(t)\\ &= \sum_{ii}\varepsilon_{ii}(\omega)+\sum_{ij,j\neq i}\varepsilon_{ij}(\omega) = \varepsilon^{auto}(\omega)+\varepsilon^{cross}(\omega) \quad (6)\\ \Delta\varepsilon(\omega) &= \mathscr{C}_{\Delta\varepsilon}\omega\sum_{ji}\int_{-\infty}^{\infty}dt e^{i(\omega+\omega_0)t}\langle\mathbf{0};d_j|\boldsymbol{\mu}_{gj}e^{-iHt/\hbar}\mathbf{m}_{ig}|d_i;\mathbf{0}\rangle f(t)\\ &= \sum_{ii}\Delta\varepsilon_{ii}(\omega)+\sum_{ij,j\neq i}\Delta\varepsilon_{ij}(\omega)\\ &= \Delta\varepsilon^{auto}(\omega)+\Delta\varepsilon^{cross}(\omega) \quad (7)\end{aligned}$$

where $\hbar\omega_0$ is the energy of the lowest vibrational state ($\mathbf{0}$) of the ground electronic state (g), and $\boldsymbol{\mu}_{gj}$ and $\mathbf{m}_{gj}$ are respectively the electric and the imaginary part of the magnetic transition dipole moments between the initial (g) and final (j) electronic states. Diabatic states are built so to be ideally independent of the nuclear coordinates. Therefore it is reasonable to assume that $\boldsymbol{\mu}_{gj}$ and $\mathbf{m}_{gj}$ do not change with coordinates (Franck-Condon approximation). $\mathscr{C}_\varepsilon$ and $\mathscr{C}_{\Delta\varepsilon}$ contain physical constants that are explicitly reported in the SI, and $f(t)$ is a damping function, either a mono-exponential or a Gaussian, corresponding in the frequency domain respectively to a Lorentzian or a Gaussian broadening. The ABS and ECD spectra can be computed by numerically propagating on the coupled PESs the so-called doorway states $|d_i;\mathbf{0}\rangle = |d_i\rangle|\mathbf{0}\rangle$ (for i=1,n), i.e. non-stationary states obtained promoting the initial vibrational state on the different diabatic excited states. In this way one can compute the terms between brackets in Eqs. 6 and 7, i.e. the auto- ($j=i$) or the cross-correlation functions ($j\neq i$). These terms are respectively collected in the "auto" $\varepsilon^{auto}(\omega)$ ($\Delta\varepsilon^{auto}(\omega)$) and "cross" $\varepsilon^{cross}(\omega)$ ($\Delta\varepsilon^{cross}(\omega)$) contributions to the spectrum. Notice that the total integral over frequencies of "cross" terms is zero, and this means that they only modulate the spectral shape without contributing to the total intensity.

Neglecting inter-state couplings, LVC model becomes equivalent to an "adiabatic" model (i.e. where inter-state couplings are not considered) known as Vertical Gradient (VG).[36] In "adiabatic" approaches, cross-correlation functions vanish and, if PESs are harmonic, the auto-correlation functions have an analytical expression,[37–40] and can be computed without the need to numerically propagate the wavepackets as done for LVC model. In this simplified approaches, the intensity-borrowing effect due to the inter-state couplings can be approximately taken into account within the perturbative HT theory,[29] allowing the transition dipoles $\boldsymbol{\mu}_{gj}$ and $\mathbf{m}_{gj}$ to have a linear dependence on the normal coordinates.[39,40]

Neglecting pre-factors $\mathscr{C}_\varepsilon$ and $\mathscr{C}_{\Delta\varepsilon}$ and the ω dependence in Eqs. 6 and 7 it is possible to analytically compute total-intensities. As it is shown in the Section S1.1.2 in the ESI, the total intensity of the spectra computed with VG at Franck-Condon (FC) level (FC|VG) is simply the sum of the dipole (ABS) or rotatory (ECD) strengths of the consdiered states and it coincides with the nonadiabatic LVC one. This points out that inter-state couplings only promote exchange of intensities. Differently, including also the HT terms (FCHT approximation), the total intensity of the VG model (FCHT|VG) is equal to the FC(LVC) one plus a new term depending on the derivatives of the transition dipoles on the normal coordinates,[41,42] which for ABS is always positive. This wrong prediction has no practical effect when the HT theory is applied to weak states well separated in energy and weakly-coupled to the states from which they borrow intensity, the original target of HT theory.[29] On the contrary, if FCHT approximation is indiscriminately applied to a dense manifold of coupled bright and dark excited states, it can introduces large artefacts.[30] In the following we show that such artefacts are dramatic for aza[7]helicene.

2.3 Decay of the lowest-excited singlet state and quantum yield of fluorescence

The lowest-excited singlet state S_1 can decay radiatively (rad) to S_0 or non-radiatively through IC to S_0 or ISC to the energetically accessible triplet states. All these processes are typically remarkably slower (ns to μs) than $S_n \rightarrow S_1$ (fs to ps). Since on this timescale the effect of quantum coherences is expected to be negligible, the calculation of the population transfer does not need a QD treatment. On the contrary the decay of the initial population of S_1 is usually described in terms of first-order kinetic rates which can be computed within FGR framework. In particular, IC or ISC rates for a transition from an initial state e_i to final state e_f (we now use the symbol "e" and not "d" to make clear that in this case we are referring to adiabatic electronic states) are obtained with the same FGR formal expression (χ=IC, ISC)

$$k_\chi(\Delta E_{if}) = \frac{2\pi}{\hbar}\sum_{r,s}\frac{e^{-\beta E_i}}{Z_i}|\langle e_i\phi_{ir}|H_\chi|e_f\phi_{fs}\rangle|^2\delta(\Delta E_{if}+E_{ir}-E_{fs}) \quad (8)$$

where ϕ_{ir} and ϕ_{fs} are the vibrational states associated to e_i and e_f, ΔE_{if} is the so called adiabatic energy difference (i.e. between the two states in their minima) and we also considered a thermal distribution of initial states at temperature T. Therefore, $\beta = 1/K_BT$, K_B is the Boltzmann constant and, finally, Z_i is the partition function of the vibrational states of the initial state i. IC and ISC are distinguished for the coupling H_χ, which is the nonadiabatic

coupling (NAC) for χ=IC and the spin orbit coupling (SOC) for χ=ISC.

Expression Eq. 8 can be conveniently translated in a TD framework obtaining

$$k_\chi(\Delta E_{if}) = \frac{1}{\hbar^2 Z_i}\int_\infty^\infty dt e^{i\Delta E_{if}t} Tr[e^{(it-\beta)H_i/\hbar} H_\chi e^{-itH_f/\hbar} H_\chi^\dagger] f(t) \quad (9)$$

where H_i and H_f are the vibrational Hamiltonians for states i and f, Tr indicates a trace over the initial vibrational states and we inserted the same damping function $f(t)$ introduced in Eqs. 6 and 7. If H_i and H_f describe harmonic motions, the trace (Tr) has an analytical expression at any temperature,[38,43] also in the case the PESs of i and f have different normal modes and frequencies (Duschinsky effect).

As far as k_{rad} from state i to g is considered, it is simply obtained from the integration over the frequency of the corresponding emission spectrum which, in fact, is defined as the rate of photon emission per unit of frequency

$$I_{rad}(\omega) = \frac{4\omega^3}{3\hbar c^3}\sum_{r,s}\frac{e^{-\beta E_r}}{Z_i}|\langle\phi_{ir}|\mu_{ig}|\phi_{gs}\rangle|^2\delta\left(\frac{\Delta E_{ig}+E_{ir}-E_{gs}}{\hbar}-\omega\right) \quad (10)$$

Also the emission spectrum can be re-written in a TD framework

$$I_{rad}(\omega) = \frac{2\omega^3}{3\pi\hbar c^3 Z_i}\int_{-\infty}^\infty dt e^{i(\Delta E_{if}-\omega)t} Tr[e^{(it-\beta)H_i/\hbar}\mu_{if}e^{-itH_f/\hbar}\mu_{fi}]f(t) \quad (11)$$

and the correlation function can be computed analytically in harmonic approximation.[38] Using the TD expression guarantees the full convergence of the spectrum calculation and therefore of the k_{rad}.

The above definitions allow to compute the fluorescence QY from the lowest-excited state S_1 ($i=1$) at temperature T defined as

$$QY_i(T) = \frac{k_{rad}}{k_{rad}+k_{IC}+\sum_f k_{ISC}(1\to f)} \quad (12)$$

where we took into account the possibility that more than one final triplet state f is energetically accessible.

We conclude this section noticing that a comparison of Eqs. 9 and 11 highlights that the calculation of k_{ISC} and k_{IC} is formally equivalent to the calculation of an emission spectrum at $\omega=0$, after substitution of the couplings H_χ with the transition dipole μ_{ig}. Alternatively, the computation of the k_{ISC} and k_{IC} can be thought to be equivalent to the calculation of an absorption spectrum at frequency $\omega=\hbar^{-1}\Delta E_{if}$ for an idealized system in which i and f electronic states have the same minimum energy. A cartoon clarifying the equivalence of the two pictures is reported in the ESI (Figure S24). The latter reading is the more straightforward one in TD calculations where one does obtain the IC/ISC rate as a function of the adiabatic energy difference (i.e. for a full family of idealized systems, obtained displacing vertically the f PES with respect to the i one), and the searched value of the rate is determined taking the value of this function at ΔE_{if} (Eq.9). The plot of the rates as a function of the energy can be interesting to analyse vibronic contributions.[44]

3 Computational details

Electronic calculations on (*M*)-aza[7]helicene were performed with density functional theory (DFT) for the ground state (GS) and TD-DFT for the excited states. We adopted CAM-B3LYP functional in combination with TZVP basis set which allowed a good agreement with the experiment for the lowest energy band of the spectrum.[28] Tests in the ESI for the excitation energies, and the oscillator and rotatory strengths with different basis sets (Table S1) confirm that TZVP is sufficiently accurate for the scopes of our study.

We used Polarizable Continuum Model (PCM) with the linear-response (LR) and state-specific (SS) implementations to describe the solvent effects on the properties of ABS and ECD spectra in CH_2Cl_2.[45–47] SS-PCM calculations were performed with Gaussian16,[48] while the rest of electronic calculations were performed with Gaussian09.[49] The "adiabatic" ABS and ECD spectra were obtained with VG model applying the TD approach[39] implemented in the version 3.0[50] of our code FCclasses.[51]

The LVC Hamiltonian was parameterized according to the method presented in ref.[31] and briefly summarized in the ESI. In order to obtain the coupling parameters $\boldsymbol{\lambda}$, the GS equilibrium structure (reference) is displaced along each normal mode and overlaps of the transition densities at the displaced and reference geometries are computed. We tested different dimensionless displacements: results with Δ= 0.1 and 0.02 have been compared in Figure S8 and are extremely similar; the value of 0.02 was used for all the calculations in present work. QD propagations were performed with the ML-MCTDH method, adopting its implementation in Quantics package.[52] We used a variable mean field (VMF) with a Runge-Kutta integrator of order 5 and accuracy 10^{-7}. Convergence tests of the ML-MCTDH propagation are reported in the ESI together with ML trees indicating the dimension of the primitive basis set and the number of single particle functions.

In order to compute the QY from the lowest-excited singlet state S_1, we considered the IC rate toward the GS and the ISC rates with all triplets whose minimum is more stable than the S_1 minimum. The S_1/S_0 NAC vector was computed at the S_1 minimum geometry with Gaussian 16.[48] We computed SOC couplings at S_1 geometry,[22,53] with TD-DFT employing ORCA 4.1.1 software package[54,55] and adopting the spin-orbit mean-field (SOMF) approximation.[56] Both radiative and non-radiative rates were computed applying the TD formalism described in section 2.3, implemented in FCclasses 3.0.[50] For these calculations we adopted the Adiabatic Hessian (AH) harmonic model,[57] in which both initial and final state PESs are expanded quadratically around their own equilibrium geometry. At variance with VG and Adiabatic Shift (AS), for which similar studies has been carried out for some [5]helicene compounds,[22] AH model also accounts for differences in normal modes (Duschinsky effect) and frequencies which have been shown to have a remarkable effect on the non-radiative rates.[58] Notice that we used a Gaussian broadening and not a Lorentzian broadening. In fact, as discussed in ref.[58], the

very long tail of the Lorentzian function can lead to artefacts where the rates, and therefore the QY, are dominated by the phenomenological broadening. In the results section we show that our estimates of the QY is robust with respect to the choice of the phenomenological Gaussian broadening.

4 Results

4.1 Electronic calculation

The purely electronic ABS and ECD spectra of aza[7]helicene computed at CAM-B3LYP/TZVP level of theory are plotted in Figure 2, summing over the first 25 electronic states in CH_2Cl_2 (LR-PCM), and 20 excited states in gas phase. Smooth spectral shapes were obtained attaching to each electronic stick line a phenomenological Gaussian with a half-width at half maximum (HWHM) of 0.25 eV. To have a more clear comparison with the experimental data, both the theoretical ABS and ECD spectra have been red-shifted by 0.4 eV. Our purely electronic spectra nicely reproduce the relative intensities of the three peaks observed experimentally in both ABS and ECD in CH_2Cl_2 at ∼3.0, ∼3.8 and ∼4.5eV. The smaller intensities predicted in gas phase improve the agreement with experiment for ABS, but worsen it for the second ECD peak. Since the experimental spectra were obtained in CH_2Cl_2,[28] in the following we will only focus on the simulation with PCM. Our results correctly capture the pattern of the signs of ECD, negative (∼3.0 eV), positive (∼3.8 eV) and negative (∼4.5 eV). The first peaks in ABS and ECD at ∼3.0 eV mainly arises from the lowest excited state S_1, while S_3-S_5 seem to contribute to the second peak at ∼3.8 eV. S_{12} is the highest-energy bright state that contribute to the experimental spectra measured up to 250 nm (∼4.96 eV) in Ref.[26]

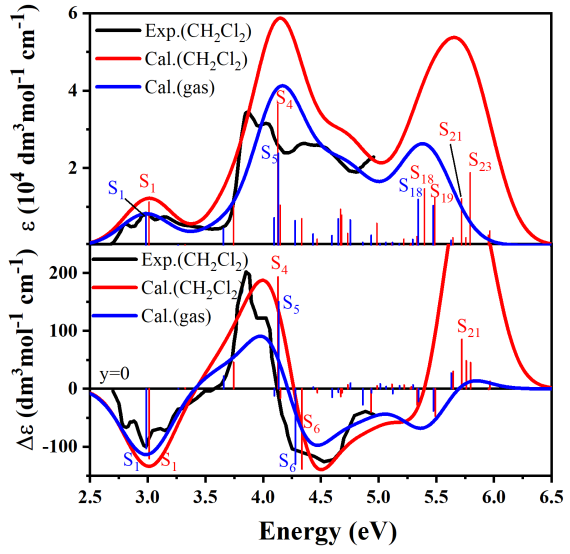

Fig. 2 Pure electronic absorption and ECD spectra of (*M*)-aza[7]helicene, obtained at CAM-B3LYP/TZVP, summing over the first 25 excited states in CH_2Cl_2 calculated with LR-PCM model and 20 excited states in gas phase, convoluted with a Gaussian with a HWHM of 0.25 eV. To have a better comparison, the theoretical spectrum has been red-shifted by 0.4 eV. The states with larger contribution to the spectra are labelled.

Table 1 Excitation energies E_{gf} (eV), oscillator strengths δOPA and rotatory strengths (in the length gauge, R(length), 10^{-40} cgs), for the first 13 lowest excited states of aza[7]helicene in CH_2Cl_2, calculated with CAM-B3LYP/TZVP. The adiabatic states are labeled as S_i (in parenthesis the usual nX label where X=A,B indicate their symmetry in Frank-Condon point and n orders the states with the same symmetry by increasing energy).

State	E_{gf}	δ_{OPA}	R(length)	Transition	Coefficient
S_1(1B)	3.41	0.22	-487.95	H→ L	0.68
S_2(2A)	3.72	0.003	4.51	H-1→L	0.62
S_3(3A)	4.14	0.21	188.45	H-2→L	0.64
S_4(4A)	4.53	0.73	791.52	H→L+1	0.61
S_5(2B)	4.55	0.21	-63.87	H-2→L+3	0.54
S_6(3B)	4.74	0.14	-566.30	H-1→ L+1	0.35
				H-3→L	0.50
S_7(5A)	4.87	0.03	-26.39	H→L+2	0.58
S_8(4B)	5.07	0.19	-53.63	H-2→L+1	0.53
S_9(6A)	5.08	0.16	-28.43	H-5→L	0.46
S_{10}(5B)	5.13	0.06	25.75	H-4→L	0.59
S_{11}(6B)	5.34	0.03	-166.18	H-1→L+2	0.58
S_{12}(7B)	5.39	0.11	20.15	H-4→L	-0.31
				H-2→L+1	0.31
				H→L+3	0.35

Data computed for these 12 states in PCM are reported in Table 1 and the corresponding molecular orbitals (MOs) are collected in Figure S10, in the ESI. Results in gas phase are very similar and given in the ESI. Orbitals contributing to the excited states in this energy range only involve the π-system, whereas no contribution from lone pairs on the nitrogen atoms is observed. Inspection of the MOs indicate that some excited states have partial charge-transfer (CT) character. In fact, several orbitals are more localized either on the benzoimidazole-like (HOMO-2 and HOMO-1 orbitals) or on the phenanthrene-like (LUMO) aromatic systems within aza[7]helicene. Therefore, we studied solvent effects by also using the SS-PCM approach, finding that the results are in general very similar to LR-PCM, apart from an overall reduction of the ABS and ECD intensities for most of the states (see ESI).

Table 1 shows that S_1 is the first bright state with an oscillator strength of 0.22 (δ_{OPA}) and rotatory strength of -487.95 (R, in 10^{-40} cgs) in CH_2Cl_2. It originates from the excitation of one electron from the highest occupied molecular orbital (HOMO, H) to the lowest unoccupied molecular orbital (LUMO, L). The second bright state (S_3) is a H-2→L transition and has some partial CT character, with a transfer of electron density from the terminal benzimidazole rings to the central phenanthroline-like fragment (see Figure S10). S_4 is dominated by the transition of H→L+1 and exhibits the strongest δ_{OPA} and positive R. The largest negative R is predicted for S_6, and it is the main responsible for the negative ECD peak at ∼4.5 eV. Similar discussion can be extended to the other excited states in both CH_2Cl_2 and gas phase with the help of Tables 1, S2 and Figures S9, S10.

A more detailed analysis and assignment of the experimental bands is not possible from Figure 2 since they exhibit a pronounced vibronic structure (this was actually proved computationally for the lowest energy band in ref.[28]) that is missing at

purely-electronic level. As a last comment, before moving to vibronic calculations, it is worthy to notice that Figure 2 suggests that S_4 and S_5 are blue-shifted $\sim$ 0.4 eV with respect to the second peak in both ABS and ECD. A better agreement would probably be possible adopting Coupled Cluster methods, since RI-CC2 has been shown to deliver good results on both the position and intensities of the excited states of a number of helicene derivatives.[59,60] Unfortunately, the application of the diabatization protocol for 12 states and 120 normal coordinates would be unfeasible at that level of theory. Luckily Figure 2 shows that apart from the above discussed shift, CAM-B3LYP is able to provide a reasonable description of the spectral shape in all the energy region covered by experiments and therefore this is the method we chose for the vibronic analysis reported in the following sections.

4.2 Adiabatic vibronic calculations

Figure 3 reports the vibrationally resolved spectra computed in CH_2Cl_2 (LR-PCM) with the FC|VG and FCHT|VG models. Spectra were convoluted with a Gaussian with a HWHM of 0.06 eV, chosen so to fit the width of the lowest-energy experimental bands and red-shifted by 0.27 eV. It is noteworthy that this value, which represents the error in our computations, is significantly smaller than what found at pure electronic level (0.4 eV), evidencing that part of the discrepancy was actually due to the lack of vibronic contributions. Both FC|VG and FCHT|VG methods nicely capture the fine structure for ABS and ECD in the region 2.75-3.50 eV. For energies $>$ 4.0 eV, FC|VG is in agreement with the experimental results, except for the energy shift already discussed. On the contrary, FCHT|VG predicts spectra by far too intense, and in fact the total ABS intensity in this region is almost 20 times larger than the FC|VG one. It has been very recently shown that

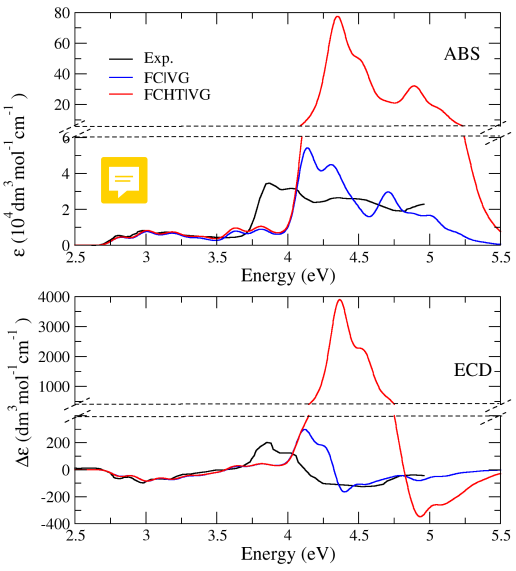

Fig. 3 Vibronic ABS (top) and ECD (bottom) spectra, obtained with VG model at 0K, summing over the first twelve excited states. The theoretical spectra are convoluted with a Gaussian with a HWHM of 0.06 eV. To have a clear comparison, the vibronic spectra have been red-shifted by 0.27 eV and scaled by a factor of 0.65.

anomalous increases of intensity predicted by FCHT with respect to FC (and LVC see below) are an artefact of the underlying perturbative approach.[30] Usually this is a minor drawback when the inter-state couplings are weak and the states well separated in energy. The 20-fold increase of the ABS intensity in aza[7]helicene, on the other side, is a perfect example to show how large this artefact can be when interacting states are very close in energy and therefore they mix remarkably. The total FC and HT intensities of ABS and ECD for the 12 excited states are reported in Table S3 and S4. The contributions of the individual states for FC|VG and FCHT|VG spectra are shown in Figure 4 and Figure S11, respectively. It is remarkable that the largest HT increase of the ABS intensity is predicted for two bright states S_4 and S_5. In Section S4.2.1 of the ESI we present an in-depth analysis based on a small 2 states-1 mode LVC model for S_4 and S_5 coupled by mode Q_{94} ($\lambda_{45}(94)$ is among the largest coupling constants). For such a model, the exact dependence of the transition dipoles on the nuclear coordinate can be computed simply by diagonalization of the LVC Hamiltonian matrix. Moving along Q_{94} (i.e. switching on the coupling), with displacements comparable to the width of the ground-state vibrational function, the states strongly mix. As expected, in the exact treatment the total intensity of the two states does not change, but the transition dipole derivatives at $Q_{94}=0$ are very large. This leads to the huge overestimation of the FCHT intensity since the HT contribution to the total intensity depends on the square module of such derivatives.[41] We clearly show that this problem arises because S_4 and S_5 are almost degenerate (energy difference of 0.0205 eV, Table 1) so that the coupling triggers a large mixing of the two states (Figure S15 in the ESI), a situation that goes well beyond what can be described with a perturbative approach. Computing the transition dipole derivatives adopting PCM in equilibrium regime we observe a much more moderate overestimation of the FCHT intensity. The 2-states model in the ESI explains this finding with the fact that the energy gap increases to 0.087 eV, so that the coupling induces a much smaller mixing of the two states and, consequently, also the derivatives of the transition dipoles are smaller.

4.2.1 Assignment of the main bands

In the low-energy region, 2.75-3.5 eV, FC|VG and FCHT|VG are very similar and show three peaks, nicely reproducing the spectral shapes of the experimental first band of both ABS and ECD. This band is attributed to the first excited state (see Figure 4) with minor contributions from the second, in agreement with what already discussed in our previous study with the models FCHT|VH and FCHT|AH.[28] The vibronic structure can be assigned to a progression along the high-frequency mode 102, a collective CC stretching sketched in Figure S19 in the ESI.

In the 3.5-3.75 eV region, the performance is generally good, but the theoretical spectra predict some ABS and ECD vibronic bands which are not seen in the experiment. An analysis of the contributions of the individual states in Figure 4 indicates that they arise mainly from S_3, with a minor contribution of S_1. It will be shown later, when the effect of interstate coupling is properly included these bands disappear. In the energy region $>$ 3.75 eV, as we mentioned above, FCHT|VG shows large artefacts. On the

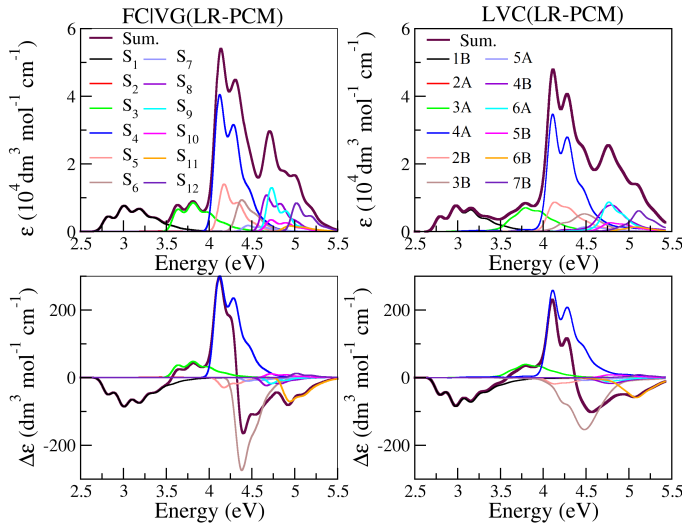

Fig. 4 The FC contribution of each states of ABS and ECD for aza[7]helicene calculated with VG and LVC model, convoluted with a Gaussian of HWHM=0.06eV. All spectra have been red-shifted by 0.27 eV and scaled by a factor of 0.65.

contrary, the agreement with experimental of the FC|VG spectrum is generally good for both the shape and intensity and allows us to identify the calculated bands at 4.07-4.37 eV with those appearing in the experiment at 3.80-4.10 eV. Therefore we can conclude that the error in the computed position of these high-energy bands is larger than for the low-energy bands.

FC|VG spectrum, indeed, reproduces reasonably well the experimental ABS and its fine structures which is attributed to the contribution of states S_4-S_6. For ECD, the positive band at 4.07-4.37 eV of ECD can be mainly attributed to the states of S_4 and S_5, and a small contribution of S_6 to ABS. Noteworthy, FC|VG spectrum reproduces the peak at 3.86 eV very well, but it fails to capture both the spectral position and width of the peak at 4.03 eV in ECD. This can be understood noticing that the signs of S_5 and S_6 are opposite to S_4 so that the mutual cancellation of their intensities leads to a steep fall for computed ECD. Notice, furthermore, that the calculated bands are more resolved than the experimental bands, especially for ABS.

4.3 LVC nonadiabatic vibronic spectra

According to our diabatization procedure,[31] the diabatic states in the LVC model coincide with the adiabatic states at the equilibrium geometry of S_0. Since they are built so to be ideally independent of the coordinates in the following, when needed, the diabatic states will be indicated with the symmetry labels (1B, 1A, 2A, ··) reported in Table 1, while adiabatic states with be specified with the usual labels (S_1, S_2, S_3 ··).

The nonadiabatic spectra calculated with LVC model are compared with experimental spectra and FC|VG results in Figure 5. LVC predicts spectra in very good agreement with the experiments and generally similar to FC|VG, showing that the effect of inter-state couplings on the spectra is only moderate. Several aspects are, however, worthy to be highlighted. Since in the low-energy region up to 3.5 eV LVC and FC|VG spectra are quite similar, a detailed comparison is given only in the ESI (Figure S17).

In the region 3.3 - 3.75 eV, LVC smoothes out the vibronic peaks predicted by FC|VG and not observed in the experiment, thus improving the agreement with experiment. In this region, the spectrum is mainly due to S_3 (3A), and the smoothing of the bands is an effect of the inter-state couplings, neglected in FC|VG . Therefore, although these couplings are small, they do have an effect on the spectral shape.

As we already noticed in the previous section, in the high-energy region, above 3.8 eV, the error in the position of the computed spectra is larger. Therefore, for easing a detailed comparison, Figure 6 shows a close up in which computed spectra are red-shifted by 0.53 eV. The two bands at ∼3.8 and ∼4.0 eV are predicted both by FC|VG and by LVC which allows a slight better accuracy for the intensity. They are assigned to a progression along modes 84 and 91. Mode 84 corresponds to a combination of CC stretching and CH bending, while mode 91 is CC and CN stretching. All those active modes are shown in Figure S19 in the ESI. Between 4.0 and 4.2 eV LVC greatly improves the agreement with experimental ECD over FC|VG, by predicting a broader and structureless spectral shape. This is mainly due to the fact that inter-state couplings give rise to broader bands and stronger mutual cancellations, which erase the 4.1 eV FC|VG band. Such couplings are mainly promoted by modes 100, 102 and 103, collective CC stretchings sketched in Figure S19 in the ESI.

In this energy region the ABS and ECD spectra arise from the contributions of S_4 (4A), S_5 (2B) and, to a minor extent, of S_3 and S_6 (3B). Actually, the diabatic states 2B and 3B exhibit the largest inter-state coupling (see Table S7 in the ESI). Their energy gap (Table 1) is comparable to the norm of their coupling,

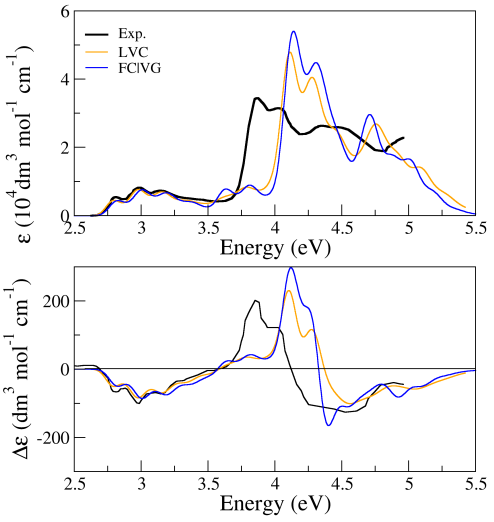

Fig. 5 Aza[7]helicene spectra of ABS (top) and ECD (bottom) computed from PCM in CH_2Cl_2 solution including 66 modes, only auto terms, during ML-MCTDH calculation, convoluted with a Gaussian of HWHM=0.06eV. Please note that all the theoretical spectra have been redshifted by 0.27 eV and scaled by a factor of 0.65.

suggesting that they strongly mix. In line with this prediction, the comparison (Figure 4) of the spectral shapes computed by FC|VC for S_6, and by LVC for the corresponding diabatic state 3B (in this case we mean the contribution arising from a wavepacket initially excited on state 3B) reveals that, according to LVC, about half of the intensity of 3B is actually transferred at lower energies in the region of 2B state (check the peak of the brown line at $\sim$ 4.25 eV). This results in a stronger mutual cancellation with the positive band at 4.2 eV arising from S_4 (4A), which ultimately leads to the correct spectral shape in this region.

While this finding highlights the importance of the inter-state couplings, comparison with FCHT|VG results (Figure 3) clearly shows that their effect cannot be described within the HT perturbative approach. A more in-depth analysis in the ESI see Section S4.2.1) put into evidence that, as expected, the same vibrational modes that carry the largest inter-state couplings, also exhibit the largest transition dipole derivatives for FCHT|VG (Table S5 in the ESI). However, while in LVC the interaction of the states just leads to a re-distribution of the total intensity, FCHT|VG predicts the huge overall intensity increase already analysed in Section 4.2. Finally, in the highest energy region ($>$ 4.5 eV), the major effect of the interstate couplings is simply a broadening of the spectral bands.

4.4 Quantum Dynamics of the fast internal conversions among the singlet excited states

The time evolution of the electronic populations of aza[7]helicene predicted by the LVC model for an initial excitation on any of the first 12 excited states is reported in Figure 7. It is worthy to highlight that since QD is run in a diabatic representation, we do report the population of the diabatic electronic states. In all cases, the population of the state initially excited decays almost completely in less than 50 fs. 1B is an expected exception, since it is significantly more stable than the other states (Table 1) and transfers only a very small fraction of its population.

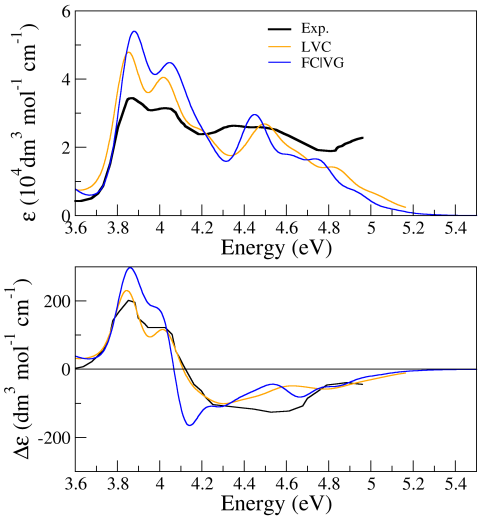

Fig. 6 aza[7]helicene spectra of ABS (top) and ECD (bottom) computed from PCM in CH_2Cl_2 solution including 66 modes, auto terms only, during ML-MCTDH calculation in high frequency region, convoluted with a Gaussian of HWHM=0.06eV. Please note that all the theoretical spectra have been redshifted by 0.53 eV and scaled by a factor of 0.65.

2A rapidly collapses to 1B, losing 90% of the initial population in $\sim$ 100 fs. At early times, 3A decays preferentially to 2A but the population of the latter is only transient and, at times $>$ 50 fs it starts flowing toward 1B. In about 100 fs, the population of 1B is already 80% and keeps growing slowly. All the other states are too far in energy to decay directly to 1B and, therefore, a cascade of internal conversions is observed, involving intermediate states. For instance, after an excitation of 4A, a rapid population transfer to 2A and 3A is observed, although 4A is actually more coupled to 1B (Table S7 in the ESI). However, the large energy gap (1.12 eV) makes a direct 4A $\rightarrow$ 1B transfer less efficient. At later times, some of the 2A population is transferred to 1B which becomes the most populated at t$>$ 200 fs. A similar dynamics is observed excitating 2B: the population decays first to 2A and 3A and only more slowly to 1B which becomes the most populated at t$>$ 550 fs.

Dynamics from 3B exhibit a particularly interesting time evolution. In fact, 3B undergoes a remarkable and ultrafast population transfer to 2B ($\sim$ 40% in less than 10 fs, see inset in Figure 7). This is due to the very strong coupling between the two states, which was previously discussed, highlighting its key role in determining the shape of the ECD spectrum.

For higher energy states (5A to 7B), the population progressively flows toward lower energy states, initially to 4A-3B and then to 2A and 3A, but on the investigated timescale, 1B is only scarcely populated. This finding is not surprising because we are running Hamiltonian dynamics and energy is conserved. A complete transfer to 1B after an initial excitation on the high-energy states would deposit a large energy amount on the vibrational modes (e.g. almost 2 eV for an excitation to 6B or 7B). This process is not efficient on the femtosecond time scale, since it would involve FC factors that are very small.

In order to describe the decay to 1B it would be necessary to account for energy dissipation, which is not trivial and is beyond the scopes of the present work. However, just to get a qualitative flavour of how this kind of ladder-type decay should take place we can reconsider the dynamics in Figure 7. In principle, the relevant dynamics after photoexcitation are those starting from bright states (those with a large oscillator strength, highlighted with bold symbols in the figure). However, Figure 7 shows that, due to nonadiabatic transitions, also almost dark states acquire some population. It is therefore interesting to inquire also if and on which timescale these dark states decay toward lower states. This is the reason why dynamics from all the considered states in the model have been reported. For instance consider 7B, the highest-energy bright state in our model. After photoexcitation its population decays in few femtoseconds, and at 700 fs, it is mainly on a group of states between 3A and 3B. The panel reporting the dynamics for an initial photoexcitation to 3A clearly shows that this state rapidly decays to 1B (S_1). The same is true for the other states, which either decay directly to 1B, or first populate 2A and

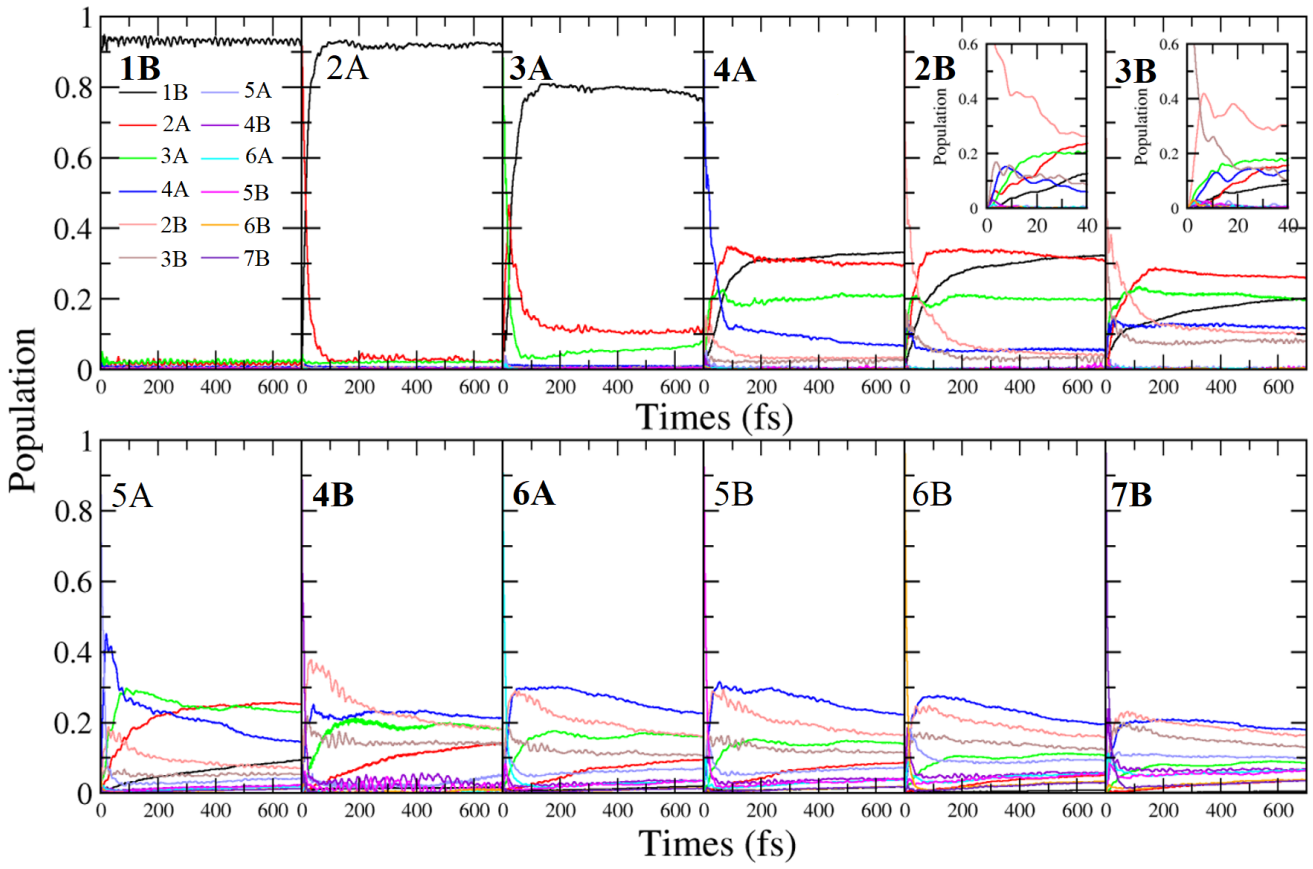

Fig. 7 Nonadiabatic dynamics of electronic diabatic populations of aza[7]helicene in CH_2Cl_2, starting from each of the diabatic states. The insets emphasize the first 40 fs. The wavepackets were propagated for 1.5 ps with ML-MCTDH, but here for better clarity results are shown for the first 700 fs (results up to 1.5 ps are in the ESI). The states with an oscillator strength > 0.1 are highlighted with bold labels.

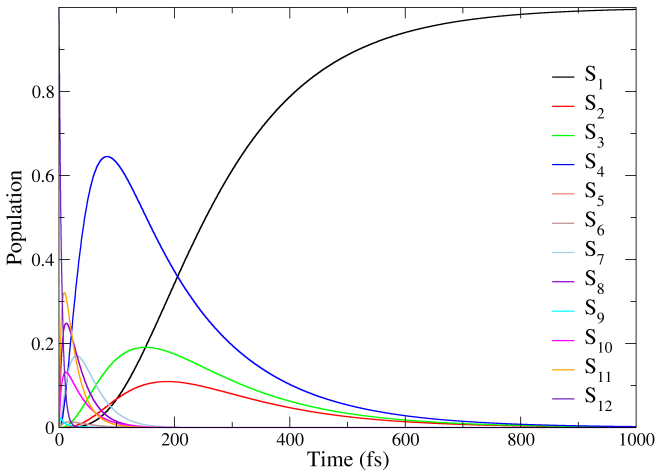

Fig. 8 Time evolution of the populations of the adiabatic states P_i as predicted by the kinetic model based for on k_{IC} rates computed with FGR. Initial conditions $P_{12}(0)$=1, $P_i(0)$=0, i=1,$\cdots$,11.

3A, which in turn, decay on 1B.

A simple alternative description of the decay to S_1 (1B) can be obtained by computing kinetic rates obtained with FGR according to Eq. 9 and then solving the kinetic model represented by following system of differential equations,

$$\frac{dP_i(t)}{dt} = -\left(\sum_{j\neq i} k_{IC}(ij)\right) P_i(t) + \sum_{j\neq i} k_{IC}(ji) P_j(t). \qquad (13)$$

In this equation, $k_{IC}(ij)$ is the kinetic rate for the $i \rightarrow j$ decay and we have an equation for the time derivative of each P_i, the population of the adiabatic state i. In this case we can explicitly consider the population of the adiabatic states S_1,$\cdots$ S_{12} exploiting the fact that their nonadiabatic couplings, necessary for applying the FGR, are easily obtained from diagonalization of the LVC model (see Section S1.3 of the ESI).

Table S9 in the ESI reports the 12×12 matrix of all the $k_{IC}(ij)$ rates computed at T=300 K with FCclasses 3.0. The time-evolution of the populations for an initial population on any of the bright states (we considered those states with an oscillator > 0.1) was computed solving the system in Eq. 13 with Mathematica 12.0. In Figure 8 we report the results for an initial population on S_{12} ($P_{12}(0)$=1); other cases are shown in Figure S23 in the ESI, and results are always qualitatively similar. It is interesting to notice that although, clearly, FGR neglects all quantum effects like interference and possibility of quantum beats, a close comparison in the ESI between QD and FGR (at T=0 K, since QD is done at this temperature) for a time-evolution starting on either S_3 (3A) or S_2 (2A), shows that FGR provides results qualitatively very similar to QD (Figure S22 in the ESI). This finding supports the reliability of FGR for these very-fast excited-state decays in aza[7]helicene. In summary, this simple approach, which does not suffer the limitations of an Hamiltonian dynamics, suggests that even starting from the highest excited state S_{12}, the excited state population fully decays to S_1 in $\sim$ 1 ps (Figure 8).

Such a $\sim$1 ps value for the flow of all excited population to S_1 should be considered only a rough lower bound. In fact, at room temperature, FGR rates implicitly assume that thermalization is faster than the IC. Probably, since ICs between excited states are predicted to be so fast, this limit is not fulfilled in aza[7]helicene, and the population of S_1 is slowed down in reality by the time needed for intra-molecular energy redistribution and dissipation to the solvent. On the grounds of time-resolved spectroscopies,[61] and theoretical models,[62] these processes are expected to occur in the sub-nanosecond timescale for common organic dyes in polar solvents. It is therefore likely that in aza[7]helicene they represent the rate limiting step for the flow of all excited population to S_1. In any case, such time scale is expected to be orders of magnitude faster than intersystem crossings and fluorescence.[63] In summary the results of this section confirm that aza[7]helicene obeys Kasha rule and the only relevant fluorescence takes place from S_1.

4.5 Decay of the lowest singlet state and fluorescence quantum yield

In this section we report the computation of QY from S_1 in CH_2Cl_2 at room temperature, considering the radiative and non-radiative (IC) decay to S_0 as well as the ISC rates to the three lowest triplet states (Table 2), since, their minima are lower in energy than S_1 one. As reported in Eq. 8, the non-radiative rates depend on the adiabatic energies between the two states involved in the transition. Moreover, the different pathways can be triggered by vibronic effects and additional precision on the calculated energies is required to reproduce possible resonances. Therefore, here in the main text we discuss results obtained from SS-PCM data for the energy differences, while results with LR-PCM and in gas-phase are given in the ESI. Differently to the ABS and ECD spectra, where both solvation models provided identical results, some differences are observed for the estimation of the QY, although they are not dramatic. Nevertheless, in all cases we observe the same order of magnitude, proving the robustness of the computational protocol.

All three T_i states correspond to $\pi\pi^*$ transitions. The SOC coupling is similar for T_2 and T_3, and remarkably smaller for T_1 (Table 2). Differences in the predicted $k_{ISC}(S_1 \rightarrow T_i)$ are however much larger than what expected from the comparison of the square of the SOC couplings and therefore must arise from vibronic effects. This point is analysed in Figure 9 where we plot the different k_{ISC} (and k_{IC}) as a function of the adiabatic energy difference, ΔE_{if}. Vertical dashed bars indicate the ΔE_{if} where the values must be taken. The logarithmic plot in the bottom panel allows the reader to directly check the value of the different rates at the intercepts with the y axis. The plots in linear scale (top and central panels), on the contrary, are given to appreciate that the rates are modulated by vibronic contributions, which are the responsible for the observed peaks. Inspection of the Figure 9 allows to conclude that the transfer $S_1 \rightarrow T_3$ is faster mainly because the ΔE_{if} is smaller and k_{ISC} is a broader function of the energy gap, due to longer vibronic progressions. More in detail, the transfer to T_3 is enhanced by the quasi-resonance with a vi-

Table 2 Excitation energies E_{gf} (eV) of the lowest excited singlet (S_i) and triplet (T_i) states, oscillator strengths δOPA for the S_0-S_i transitions and their assignments in terms of molecular orbitals. Adiabatic energy difference with respect to S_1 (ΔE_{if}), SOC and ISC rate constants ($k_{ISC}/10^7$) from S_1 to each of the three lowest energy triplets (T = 300K, HWHM = 0.06 eV). All the data are obtained at S_1 minimum energy geometry with SS-PCM in the equilibrium except SOC couplings obtained with LR-PCM.

	S_i		T_i				
State	E_{gf}	δOPA	E_{gf}	Transition	ΔE_{if} (eV)	SOC (cm^{-1})	$k_{ISC}/10^7$ (s^{-1})
1	2.71	0.18	1.37	H→L	0.96	0.22	0.003
2	3.36	0.00	2.32	H-1→L H→L+1	0.53	0.45	1.21
3	3.51	0.12	2.84	H-2→L H-1→L	0.19	0.52	7.44

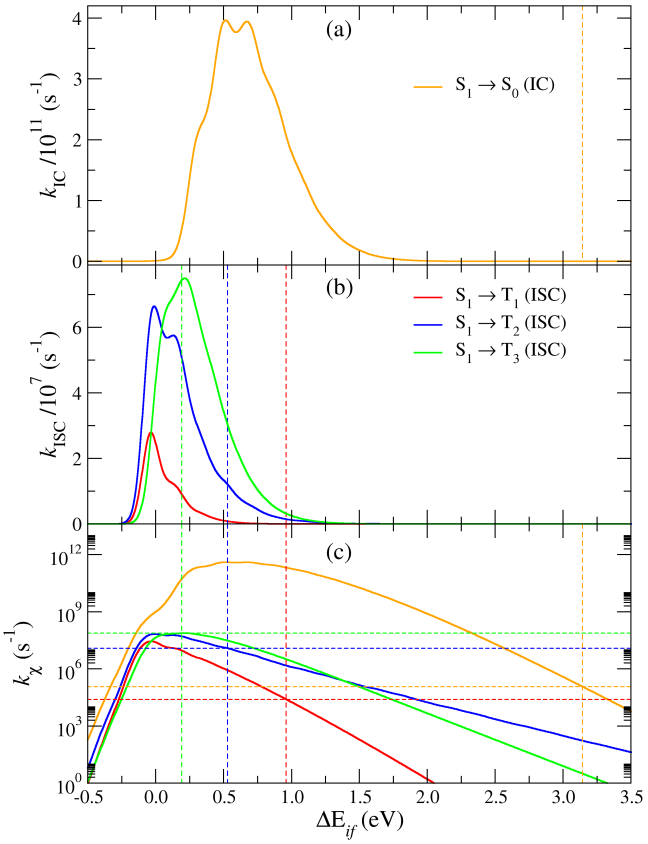

Fig. 9 Calculation of rates of non-radiative decays of S_1: (a) k_{IC} for $S_1 \rightarrow S_0$ transition as a function of the adiabatic energy difference (ΔE_{if}). (b) k_{ISC} for $S_1 \rightarrow T_i$ transitions ($i = 1,2,3$) as a function of ΔE_{if}. (c) Same plots as those reported in panels (a) and (b) but with the y-axis given in logarithmic scale. NAC and SOC couplings were computed at the S_1 minimum energy geometry. Calculations were performed at T=300K with the AH vibronic model on the grounds of PES computed with LR-PCM. Adiabatic energy differences refined at SS-PCM level. The vertical lines represent the ΔE_{if} for the $S_1 \rightarrow S_0$ (orange) and $S_1 \rightarrow T_i$ (red, blue, green) non-radiative processes, while the horizontal lines are just added to facilitate the direct reading of the rates at the intercepts with the y axis.

bronic state with 1 quantum on a T_3 mode that is analogous to mode 102 of S_0. On the contrary, the transfer to T_2 is enhanced by the (weaker) transition to the vibronic state with two quanta on a T_2 mode equivalent to S_0 mode 105. Both modes are sketched in Figure S19 of the ESI.

In summary, the $S_1 \rightarrow T_3$ intersystem crossing rate is six times faster than $S_1 \rightarrow T_2$ and both are three order of magnitude larger that the ISC rate $S_1 \rightarrow T_1$. The radiative constant k_{rad} is in the same order of magnitude than the ISC rates $S_1 \rightarrow T_2$ and $S_1 \rightarrow T_3$, and much larger than the IC rate $S_1 \rightarrow S_0$, which is two order of magnitude smaller (Table 3).

Considering these data, a quantum yield $QY^{cal} = 0.38$ is predicted, in excellent agreement with the experimental value $QY^{exp} = 0.39$. As we pointed out in Section 2.3, k_{IC} and k_{ISC} both depend, in principle, on the damping function (the broadening in the frequency domain) and the computed ΔE_{if}. For what concerns the broadening, the above values were obtained considering a Gaussian lineshape with HWHM=0.06 eV, where this value was chosen because it allows a good reproduction of the width of the spectral bands in the previous figures. However, in Table 3 we show that our estimate of the QY is robust with respect to different reasonable choices of the broadening. In fact QY ranges between 0.36-0.39 for HWHM from 0.01-0.10 eV.

Figure 9 highlights how much the rates are sensitive to ΔE_{if}, which, in turn depends on the computational protocol and, for instance, on how solvent effects are described. In the SI we discuss in detail the results in gas phase and using LR-PCM. Although some changes are observed, the estimated QY does not vary remarkably, allowing us to conclude that the partial quenching of the fluorescence of aza[7]helicene is due to ISC to low-energy triplet states.

5 Conclusion

In this wcontribution we reported an extensive computational analysis of vibronic effects in the photophysics of aza[7]helicene. We analysed the shape of the absorption and ECD spectra, the cascade of internal conversions among the excited singlet states and, finally, the rates of the radiative and non radiative processes that depopulate the lowest-energy singlet state S_1, determining the quantum yield of fluroescence.

We adopted a LVC model parametrized with TD-DFT and ML-MCTDH wavepacket propagations for the computation of the nonadiabatic vibronic spectra and the ultrafast nonadiabatic dynamics. On the other side, we used vibronic approaches based on Fermi Golden rule and analytical correlation functions for the computation of the spectra neglecting the non-adiabatic couplings, as well as for the computation of the kinetic rates for the decay of S_1.

Concerning the spectroscopy, accounting for vibronic contribu-

Table 3 Fluorescence quantum yields QY= k_{rad}(k_{rad}+ k_{IC}+k_{ISC})$^{-1}$ of aza[7]helicene, calculated with AH model. A Gaussian broadening function with different value of HWHM$_G$ was used, and the contribution of all the triplets is included in k_{ISC}. T = 300K.

Broadening (HWHM, eV).	$k_{rad}/10^7$ (s^{-1})	$k_{IC}/10^7$ (s^{-1})	$k_{ISC}/10^7$ (s^{-1})	QY^{cal} (QY^{exp} = 0.39))
0.01	5.25	0.025	9.24	0.36
0.02	5.25	0.025	9.18	0.36
0.03	5.25	0.025	9.02	0.37
0.04	5.25	0.025	8.88	0.37
0.05	5.25	0.025	8.75	0.37
0.06	5.25	0.025	8.65	0.38
0.10	5.25	0.029	8.28	0.39

tions of the 12 lowest-energy states we achieved a confident assignment of all the main features of the entire experimental spectra up to 250nm, covering a frequency range $>$ 2 eV. Vibronic spectra obtained at FC|VG and FCHT|VG are in nice agreement with experiment in low energy region of 2.75-3.5 eV, where the effect of inter-state couplings is weak. Above 3.5 eV, a proper introduction of the effect of inter-state couplings with the LVC model improves the agreement with experiment. Although their effect is generally moderate and limited to a broadening of the bands, in some cases they wash out computed bands that, in fact, are not observed in the experiment.

Interestingly, we show that aza[7]helicene provides a remarkable example of the breakdown of Herzberg-Teller perturbative approximation, due to the fact that above 3.5 eV the electronic states are coupled and very close to each other. Such a breakdown in fact manifests with dramatic artefacts, like an erroneous increase of the predicted absorption intensity by a factor 20.

Quantum dynamics wave packet propagations show that all bright states decay in less than 50 fs. While low-lying states fully decay, in a direct or indirect way, to S_1, QD predicts that the populations of higher energy states initially distribute on several intermediate states. Hamiltonian dynamics without dissipation effects cannot describe the subsequent flow of the population to S_1. A simple kinetic model based on Fermi Golden rule sets a lower bound of 1 picosecond to the timescale for the complete transfer of population from all singlet states to S_1. This finding suggests that the rate limiting step for such process is actually the dissipation of energy with the environment, a process expected to occur on the sub-ns timescale.

The computed quantum yield of fluorescence from S_1 perfectly matches the experimental measurement, and allows us to conclude that the fluorescence of aza[7]helicene is quenched by 60% due to the competition between the radiative decay and the intersystem crossings to the lowest-energies triplet states.

On more general grounds, we believe that the results here presented document the potentiality of the adopted approach based on LVC models and a combination of QD simulations and kinetic rates models to shed light on the details of the photophysics of semi-rigid dyes of remarkable technological interest like helicenes.

Conflicts of interest

There are no conflicts to declare

Acknowledgements

We thank the project supported by the National Natural Science Foundation of China (Grant No. 11904149). DA acknowledges Fundación Ramón Areces (Spain) for funding his postdoctoral stay at ICCOM-CNR Pisa. The authors thank Javier Cerezo (Universidad Autónoma de Madrid) for helpful discussions on the computation of quantum yields.

Notes and references

1 Y. Shen and C. F. Chen, *Chem. Rev.*, 2012, **112**, 1463–1535.

2 M. Gingras, *Chem. Soc. Rev.*, 2013, **42**, 968–1006.

3 S. Grimme, J. Harren, A. Sobanski and F. Vögtle, *Eur. J. Org. Chem.*, 1998, **1998**, 1491–1509.

4 M. Srebro, E. Anger, B. M. II, N. Vanthuyne, C. Roussel, R. Réau, J. Autschbach and J. Crassous, *Chem. - Eur. J.*, 2015, **21**, 17100.

5 N. J. Schuster, R. H. Sanchez, D. Bukharina, N. A. Kotov, N. Berova, F. Ng, M. L. Steigerwald and C. Nuckolls, *J. Am. Chem. Soc.*, 2018, **140**, 6235–6239.

6 T. Mori, *Chem. Rev.*, 2021, DOI: 10.1021/acs.chemrev.0c01017.

7 N. J. Schuster, R. Herández Sánchez, D. Bukharina, N. A. Kotov, N. Berova, F. Ng, M. L. Steigerwald and C. Nuckolls, *J. Am. Chem. Soc.*, 2018, **140**, 6235–6239.

8 N. J. Schuster, L. A. Joyce, D. W. Paley, F. Ng, M. L. Steigerwald and C. Nuckolls, *J. Am. Chem. Soc.*, 2020, **142**, 7066–7074.

9 X. Xiao, S. K. Pedersen, D. Aranda, J. Yang, R. A. Wiscons, M. Pittelkow, M. L. Steigerwald, F. Santoro, N. J. Schuster and C. Nuckolls, *J. Am. Chem. Soc.*, 2021, **143**, 983–991.

10 J. Y. Koo, Y. Yakiyama, G. R. Lee, J. Lee, H. C. Choi, Y. Morita and M. Kawano, *J. Am. Chem. Soc.*, 2016, **138**, 1776–1779.

11 R. H. Janke, G. Haufe, E.-U. Würthwein and J. H. Borkent, *J. Am. Chem. Soc.*, 1996, **118**, 6031–6035.

12 Y. Yang, R. C. Da Costa, M. J. Fuchter and A. J. Campbell, *Nat. Photonics*, 2013, **7**, 634–638.

13 C. Schaack, L. Arrico, E. Sidler, M. Górecki, L. Dibari and F. Diederich, *Chem. - Eur. J.*, 2019, **25**, 8003–8007.

14 M. T. Reetz and S. Sostmann, *Tetrahedron*, 2001, **57**, 2515–2520.

15 J. Birks, D. Birch, E. Cordemans and E. Vander Donckt, *Chem. Phys. Lett.*, 1976, **43**, 33–36.

16 O. Weigang Jr, J. Turner and P. Trouard, *J. Chem. Phys.*, 1966, **45**, 1126–1134.

17 E. Vander Donckt, J. Nasielski, J. Greenleaf and J. Birks, *Chem. Phys. Lett.*, 1968, **2**, 409–410.

18 H. Sakai, T. Kubota, J. Yuasa, Y. Araki, T. Sakanoue, T. Takenobu, T. Wada, T. Kawai and T. Hasobe, *J. Phys. Chem. C*, 2016, **120**, 7860–7869.

19 M. Sapir and E. V. Donckt, *Chem. Phys. Lett.*, 1975, **36**, 108–110.

20 N. I. Nijegorodov and W. S. Downey, *J. Phys. Chem.*, 1994, **98**, 5639–5643.

21 D. Beljonne, Z. Shuai, G. Pourtois and J. Bredas, *J. Phys. Chem. A*, 2001, **105**, 3899–3907.

22 K. Schmidt, S. Brovelli, V. Coropceanu, D. Beljonne, J. Cornil, C. Bazzini, T. Caronna, R. Tubino, F. Meinardi, Z. Shuai *et al.*, *J. Phys. Chem. A*, 2007, **111**, 10490–10499.

23 M. Gingras, G. Félix and R. Peresutti, *Chem. Soc. Rev.*, 2013, **42**, 1007–1050.

24 S. Zheng, J. Lan, S. I. Khan and Y. Rubin, *J. Am. Chem. Soc*, 2003, **125**, 5786–5791.

25 R. Berger, A. Giannakopoulos, P. Ravat, M. Wagner, D. Beljonne, X. Feng and K. Müllen, *Angew. Chem., Int. Ed.*, 2014, **53**, 10520–10524.

26 T. Otani, A. Tsuyuki, T. Iwachi, S. Someya, K. Tateno, H. Kawai, T. Saito, K. S. Kanyiva and T. Shibata, *Angew. Chem., Int. Ed. Engl.*, 2017, **56**, 3906–3910.

27 K. Uematsu, K. Noguchi and K. Nakano, *Phys. Chem. Chem. Phys.*, 2018, **20**, 3286–3295.

28 Y. Liu, Q. Xu, S. Jie, L. Wang, D. He, M. Wang and C. Yang, *Spectrochim. Acta, Part A*, 2020, **239**, 118475.

29 G. Herzberg and E. Teller, *Z. Phys. Chem. B*, 1933, **21**, 410.

30 D. Aranda and F. Santoro, *J. Chem. Theory Comput.*, 2021, accepted, DOI: 10.1021/acs.jctc.1c00022.

31 M. Yaghoubi Jouybari, Y. Liu, R. Improta and F. Santoro, *J. Chem. Theory Comput.*, 2020, **16**, 5792–5808.

32 H. Wang and M. Thoss, *J. Chem. Phys.*, 2003, **119**, 1289–1299.

33 U. Manthe, *J. Chem. Phys.*, 2008, **128**, 164116.

34 U. Manthe, *J. Chem. Phys.*, 2009, **130**, 054109.

35 O. Vendrell and H.-D. Meyer, *J. Chem. Phys.*, 2011, **134**, 044135.

36 F. J. Avila Ferrer and F. Santoro, *Phys. Chem. Chem. Phys.*, 2012, **14**, 13549.

37 R. Ianconescu and E. Pollak, *J. Phys. Chem. A*, 2004, **108**, 7778–7784.

38 Q. Peng, Y. Niu, C. Deng and Z. Shuai, *Chem. Phys.*, 2010, **370**, 215–222.

39 F. J. Avila Ferrer, J. Cerezo, J. Soto, R. Improta and F. Santoro, *Comput. Theor. Chem.*, 2014, **1040**, 328–337.

40 J. Huh and R. Berger, *J. Phys.: Conf. Ser.*, 2012, **380**, 012019.

41 F. Santoro, A. Lami, R. Improta, J. Bloino and V. Barone, *J. Chem. Phys.*, 2008, **128**, 224311.

42 N. Lin, Y. Luo, F. Santoro, X. Zhao and A. Rizzo, *Chemical Physics Letters*, 2008, **464**, 144 – 149.

43 M. Etinski, V. Rai-Constapel and C. M. Marian, *J. Chem. Phys.*, 2014, **140**, 114104.

44 For k_{ISC} and especially k_{IC} the adoption of TD expressions is particularly convenient since, due to energy-conservation, they depend on transitions to a dense manifold of final states with strong vibrational excitation (on the order of ΔE_{if}, which is usually very large especially for IC). In a spectrum calculation, this would correspond to take values in the long and very weak tail far from the 0-0 transition. This region of the spec-

trum challenges TI approaches, while it is easily computed with TD approaches, which guarantee full convergence. The involvement of highly excited vibrational states highlight that harmonic approximation could be critical for k_{IC} and k_{ISC}. This possible issue has been recently investigated.[58,64].

45 J. Tomasi, B. Menucci and R. Cammi, *ChemInform*, 2005, **36**, 2999–3094.

46 R. Improta, V. Barone, G. Scalmani and M. J. Frisch, *J. Chem. Phys.*, 2006, **125**, 054103.

47 R. Improta, G. Scalmani, M. J. Frisch and V. Barone, *J. Chem. Phys.*, 2007, **127**, 074504.

48 M. J. Frisch, G. W. Trucks, H. B. Schlegel, G. E. Scuseria, M. A. Robb, J. R. Cheeseman, G. Scalmani, V. Barone, G. A. Petersson, H. Nakatsuji, X. Li, M. Caricato, A. V. Marenich, J. Bloino, B. G. Janesko, R. Gomperts, B. Mennucci, H. P. Hratchian, J. V. Ortiz, A. F. Izmaylov, J. L. Sonnenberg, D. Williams-Young, F. Ding, F. Lipparini, F. Egidi, J. Goings, B. Peng, A. Petrone, T. Henderson, D. Ranasinghe, V. G. Zakrzewski, J. Gao, N. Rega, G. Zheng, W. Liang, M. Hada, M. Ehara, K. Toyota, R. Fukuda, J. Hasegawa, M. Ishida, T. Nakajima, Y. Honda, O. Kitao, H. Nakai, T. Vreven, K. Throssell, J. A. Montgomery, Jr., J. E. Peralta, F. Ogliaro, M. J. Bearpark, J. J. Heyd, E. N. Brothers, K. N. Kudin, V. N. Staroverov, T. A. Keith, R. Kobayashi, J. Normand, K. Raghavachari, A. P. Rendell, J. C. Burant, S. S. Iyengar, J. Tomasi, M. Cossi, J. M. Millam, M. Klene, C. Adamo, R. Cammi, J. W. Ochterski, R. L. Martin, K. Morokuma, O. Farkas, J. B. Foresman and D. J. Fox, *Gaussian~16 Revision B.01*, 2016, Gaussian Inc. Wallingford CT.

49 M. J. Frisch, G. W. Trucks, H. B. Schlegel, G. E. Scuseria, M. A. Robb, J. R. Cheeseman, G. Scalmani, V. Barone, G. A. Petersson, H. Nakatsuji, X. Li, M. Caricato, A. V. Marenich, J. Bloino, B. G. Janesko, R. Gomperts, B. Mennucci, H. P. Hratchian, J. V. Ortiz, A. F. Izmaylov, J. L. Sonnenberg, D. Williams-Young, F. Ding, F. Lipparini, F. Egidi, J. Goings, B. Peng, A. Petrone, T. Henderson, D. Ranasinghe, V. G. Zakrzewski, J. Gao, N. Rega, G. Zheng, W. Liang, M. Hada, M. Ehara, K. Toyota, R. Fukuda, J. Hasegawa, M. Ishida, T. Nakajima, Y. Honda, O. Kitao, H. Nakai, T. Vreven, K. Throssell, J. A. Montgomery, Jr., J. E. Peralta, F. Ogliaro, M. J. Bearpark, J. J. Heyd, E. N. Brothers, K. N. Kudin, V. N. Staroverov, T. A. Keith, R. Kobayashi, J. Normand, K. Raghavachari, A. P. Rendell, J. C. Burant, S. S. Iyengar, J. Tomasi, M. Cossi, J. M. Millam, M. Klene, C. Adamo, R. Cammi, J. W. Ochterski, R. L. Martin, K. Morokuma, O. Farkas, J. B. Foresman and D. J. Fox, *Gaussian~09 Revision A.02*, 2009, Gaussian Inc. Wallingford CT.

50 F. Santoro and J. Cerezo, *FCclasses3, a code for vibronic calculations. Available upon request*, 2019.

51 F. Santoro, *FCclasses, a Fortran 77 code, visit: www.pi.iccom.cnr.it/fcclasses*, 2020.

52 G. A. Worth, K. Giri, G. W. Richings, M. H. Beck, A. Jäckle and H.-D. Meyer, *The QUANTICS Package, Version 1.1, (2015), University of Birmingham, Birmingham, U.K.*

53 L. AbadGalán, J. M. Castán, ClémentDalinot, P. SimónMarqués, PhilippeBlanchard, OlivierMaury, ClémentCabanetos, T. L. Bahers and CyrilleMonnereau, *Phys. Chem. Chem. Phys.*, 2020, **22**, 12373–12381.

54 F. Neese, *Software update: the ORCA program system, Version 4.1.1,WIREs Comput Mol Sci 2018, 8, e1327. doi: 10.1002/wcms.1327*.

55 *ORCA, the ORCA program system, Version 4.1.1, visit: https://orcaforum.kofo.mpg.de/app.php/portal*.

56 F. Neese, *J. Chem. Phys.*, 2005, **122**, 1847.

57 F. J. Avila Ferrer and F. Santoro, *Phys. Chem. Chem. Phys.*, 2012, **14**, 13549–13563.

58 A. Humeniuk, M. Bužančić, J. Hoche, J. Cerezo, R. Mitrić, F. Santoro and V. Bonačić-Kouteckỳ, *J. Chem. Phys.*, 2020, **152**, 054107.

59 Y. Nakai, T. Mori and Y. Inoue, *J. Phys. Chem. A*, 2012, **116**, 7372–7385.

60 Y. Nakai, T. Mori, K. Sato and Y. Inoue, *J. Phys. Chem. A*, 2013, **117**, 5082–5092.

61 M. L. Horng, J. A. Gardecki, A. Papazyan and M. Maroncelli, *J. Phys. Chem.*, 1995, **99**, 17311–17337.

62 V. B. Jr, T. Wei, D. D. Tommaso, D. Abramavicius, J. Hauer, T. Polívka and C. D. P. Duffy, *Chem Sci*, 2019, **10**, 4792–4804.

63 For the brightest state, S_4, according to the treatment described in Section 2.3 k_r is predicted to be $\sim 3.5\ 10^8\ s^{-1}$.

64 R. R. Valiev, R. T. Nasibullin, V. N. Cherepanov, G. V. Baryshnikov, D. Sundholm, H. Ågren, B. F. Minaev and T. Kurtén, *Phys. Chem. Chem. Phys.*, 2020, **22**, 22314–22323.

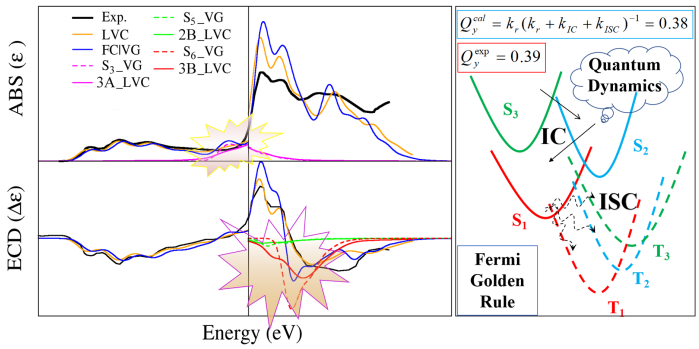
Exp.
LVC
FCIVG
S3_VG
3A_LVC
S5_VG
2B_LVC
S6_VG
3B_LVC
ABS (ε)
ECD (Δε)
Energy (eV)
$Q_y^{cal} = k_r(k_r + k_{IC} + k_{ISC})^{-1} = 0.38$
$Q_y^{exp} = 0.39$
Quantum Dynamics
S3
IC
S2
ISC
S1
T3
T2
T1
Fermi Golden Rule